ELSEVIER

Journal of Alloys and Compounds 275–277 (1998) 424–429

Journal of ALLOYS AND COMPOUNDS

Energy levels and crystal field calculations of Nd^{3+} in the $REBMO_5$ phases (RE=rare earth, M=Ge, Si)

E. Antic-Fidancev[a,*], M. Lemaitre-Blaise[a], M. Taibi[b], J. Aride[b], A. Boukhari[c], P. Porcher[a]

[a]*Laboratoire de Chimie Métallurgique et Spectroscopie des Terres Rares, CNRS, 1, Place Aristide Briand, 92195 Meudon, France*
[b]*Laboratoire de Physico–Chimie des Matériaux, Laboratoire Associé Francophone AUPELF-UREF (LAF 502), E.N.S, B.P 5118 Takaddoum, Rabat, Morocco*
[c]*Laboratoire de Chimie du Solide Appliquée, Laboratoire Associé Francophone AUPELF-UREF (LAF 501), Faculté des Sciences, B.P 1014 Avenue Ibn Battouta, Rabat, Morocco*

Abstract

The optical properties of mixed oxides from the RE_2O_3–B_2O_3–MO_2 chemical system (RE=rare earth; M=Ge, Si) with general formula $REBMO_5$ have been analyzed. The energy level scheme of the Nd^{3+} ion in the two structural types $NdBGeO_5$ and $NdBSiO_5$ have been deduced from the absorption and emission spectra recorded at different temperatures between 4.2 and 300 K. The simulation has been carried out on the 109 energy levels found for $NdBGeO_5$ and 125 for $NdBSiO_5$. The phenomenological crystal field parameters have been determined assuming a C_{2v} point symmetry for the rare earth in $NdBGeO_5$ and C_2 or C_s in $NdBSiO_5$. The r.m.s. standard deviation is 17.5 cm^{-1} for $NdBGeO_5$ and 18.1 cm^{-1} for $NdBSiO_5$, indicating a satisfying agreement between the calculated and experimental levels. © 1998 Elsevier Science S.A.

Keywords: Trigonal phases; Mixed oxides

1. Introduction

In the last few years a great effort has been carried out on the synthesis and on the spectroscopic properties of rare earth borogermanates and silicates. This interest is the consequence of their potential application as effective self-frequency-doubling mini-lasers. Alexsander Kaminskii and his group were the first to grow single crystals of the trigonal acentric $LaBGeO_5$ doped with Pr^{3+} and Nd^{3+}. They discovered that this crystal is a new nonlinear crystal laser, after $LiNbO_3$:Mg^{2+} and $YAl_3(BO_3)_4$:Nd^{3+} [1–4].

Recently, we have published the luminescence properties of the Eu^{3+} ion embedded in the two $REBGeO_5$ varieties [5]. In the stillwellite type structure of $LaBGeO_5$:Eu^{3+} a large value of the second rank crystal field parameters (cfp) were found. This was a consequence of the unusually large $^7F_1$ splitting, one of the largest splittings we have ever observed for compounds doped with Eu^{3+}. The second rank crystal field strength parameter has the same magnitude as found for the S_6 site of the C-type oxide [6] or for the apatite [7].

However, one of the most popular RE^{3+} ions used as a spectroscopic tool is Nd^{3+}, with $4f^3$ configuration which, at the same time, offers both the maximum amount of interactions to be characterized and still a relatively simple and conveniently reproducible set of observed energy levels among the 182 Kramers' doublets. This is why the present work deals with the report of the Nd^{3+} optical properties in both $REBMO_5$ structural varieties. Due to the important potential application it seemed interesting to simulate the energy levels schemes, using a crystal field potential as close as possible to the real point symmetry.

2. Crystallographic background

The $REBMO_5$ compounds (RE=Rare Earth; M=Ge, Si) have been synthesized from high purity RE_2O_3, H_3BO_3 and MO_2 oxides. The stoichiometric mixture of starting materials is ground and heated first at 400°C for a few hours. A progressive heating treatment is thus carried out at 850°C during 24 h in order to avoid any loss of H_3BO_3. The resulting compound is ground again and heated for a further 24 h period at 1100°C. The purity and homogeneity of the obtained products have been controlled by a routine X-ray diffraction technique.

*Corresponding author.

PII: S0925-8388(98)00361-2

Two crystallographic structures have been identified for $REBGeO_5$ depending on the rare earth size. For lanthanides with larger ionic radii (RE=La, Pr and Nd in the low temperature phase), $REBGeO_5$ crystallizes with the stillwellite structural type (the generic compound is $CeBSiO_5$). The cell symmetry is trigonal with C_3^2–$P3_1$ (No. 144 in [8]) as space group [9–15]. The rare earth occupies a site of low point symmetry, C_1, and is coordinated to nine oxygens. The La–O distances vary between 2.407 and 2.742 Å (av. 2.605 Å). The germanium and boron atoms are located at the center of a distorted tetrahedra whose connections form helical chains along the *c*-axis. From Nd (high temperature phase) to Er, another structural type was found for the rare earth borogermanates. They are isotypic with the datolite type structure (the generic compound is $CaBSiO_4OH$). The cell symmetry is monoclinic and the space group is C_{2h}^5–$P2_1/c$ (No. 14 in [8]), [13,16]. The datolite structure is layered and the larger cations are separated by BO_4 and GeO_4 tetrahedra. In this structure, the rare earth is located at the center of a distorted Thompson cube of coordination. The point symmetry is also low, C_1. In $NdBGeO_5$ the Nd–O distances are comprised between 2.345 and 2.560 Å (av. 2.470 Å). These distances are shorter than those observed in the lanthanum compound, a consequence of the lanthanidic contraction. Moreover, the $^7F_1$ splitting of $GdBGeO_5$:Eu^{3+} suggests a symmetry close to a higher one [5]. For the rest of the series (RE=Tm, Yb, Lu), the stoichiometry does not exist and the rare earth pyrogermanate $RE_2Ge_2O_7$ appears to be the stable phase in the synthesis stage.

3. Spectroscopic analysis

The absorption spectra were measured at different temperatures (9–300 K) in order to vary the population rate of the ground level crystal field states. They were recorded through a double beam Cary 2400 spectrophotometer, equipped with a helium cryopump. The emission spectrum of $NdBGeO_5$ is excited when the sample is directly immersed in the liquid helium, at 4.2 K. The spectrum is analyzed through a 1 m monochromator (Jobin–Yvon) equipped with a standard detector (Hamamatsu R306).

3.1. Monoclinic phase $NdBGeO_5$

The absorption spectrum of $NdBGeO_5$ recorded at 9 K in the UV-visible–near IR domain consists of almost only sharp lines easily assigned to the electronic transitions. For the $^4I_{9/2}\rightarrow{}^2P_{1/2}$ transition, which is well isolated in the spectrum, only one absorption line is observed. This indicates a rare earth located in a single site, in agreement with the crystallographic data. The energy position of $^2P_{1/2}$

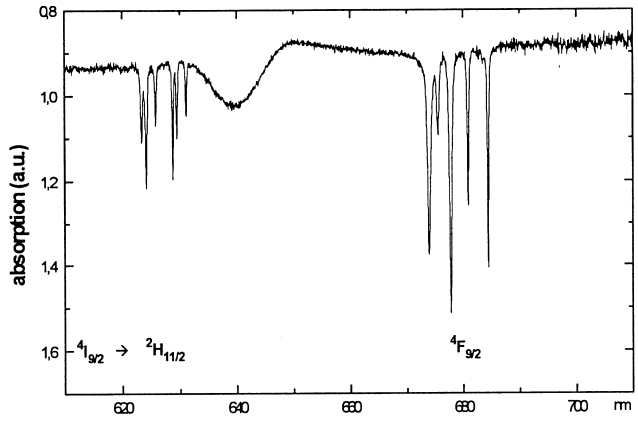

Fig. 1. Part of the absorption spectrum of $NdBGeO_5$, recorded at 9 K. The large band at 640 nm is due to a change of detector.

locates $NdBGeO_5$ in the eigthfold coordinated compounds area in the nephelauxetic scale [17,18]. At room temperature, five distinct lines are observed for $^4I_{9/2}\rightarrow{}^2P_{1/2}$ corresponding to transitions from the crystal field components of the ground level. These components are situated, respectively, at 0, 123, 195, 321 and 395 cm^{-1}. This is due to the fact that $^2P_{1/2}$ is not split by the crystal field. The relatively high energy of the second crystal field levels indicates that absorption measurements below 9 K are not necessary, in terms of population rate. Fig. 1 presents a part of the absorption spectrum recorded at 9 K in the 610–690 nm wavelength range corresponding to the transition towards $^2H_{11/2}$ and $^4F_{9/2}$ levels. All crystal field levels are unambiguously observed for both transitions.

The emission spectrum of $NdBGeO_5$ recorded at 4.2 K comprises a great number of narrow lines provided from several emitting levels ($^4D_{3/2}$: 27 864 cm^{-1}, $^2P_{3/2}$: 26 069 cm^{-1}, $^4G_{7/2}$: 18 882 cm^{-1} and $^4G_{5/2}$: 16 998 cm^{-1}). Emission from $^4D_{3/2}$ permits the deduction of the $^4I_{9/2}$ and $^4I_{11/2}$ manifolds.

From these absorption and emission measurements an energy level scheme of 109 levels among the 182 Kramers' doublets of the $4f^3$ configuration was constructed.

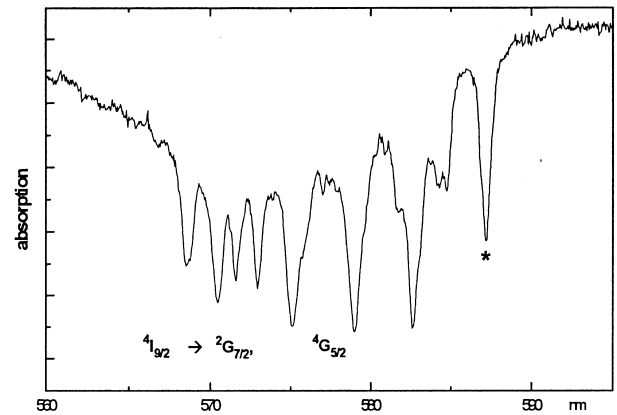

Fig. 2. $^4I_{9/2}\rightarrow{}^4G_{5/2}$, $^2G_{7/2}$ transitions in $NdBSiO_5$.

3.2. Trigonal phases

The absorption spectra of $NdBSiO_5$ and $La_{0.4}Nd_{0.6}BGeO_5$ compounds owing to the trigonal phase of the borogermanates were recorded at 9 K. They clearly show that Nd^{3+} occupies a single crystallographic site. The high energy observed for $^2P_{1/2}$ in the nephelauxetic scale: 23 367 cm^{-1} (resp. 23 373 cm^{-1}) for $NdBSiO_5$ (resp. for $La_{0.4}Nd_{0.6}BGeO_5$) confirms that the rare earth coordination is higher than for the monoclinic phase, i.e. in the ninefold coordinated compounds area of the nephelauxetic scale [17,18]. This is in agreement with the crystallographic structure in which a structural skeleton formed by REO_9 polyhedra can be identified. In the absorption spectrum of $La_{0.4}Nd_{0.6}BGeO_5$ the presence of the monoclinic $NdBGeO_5$ phase is also observed as an impurity. This shows that the limit of the $La_{1-x}Nd_xBGeO_5$ solid solution system in its trigonal form is probably situated for x lower than 0.6, although it is not proven from the X-ray diffraction patterns. In the following description and simulation only the optical data of $NdBSiO_5$ will be retained.

Table 1
Experimental and calculated energy levels of $NdBGeO_5$

$^{2S+1}L_J$ level	E (exp.)	E (calc.)	$^{2S+1}L_J$ level	E (exp.)	E (calc.)	$^{2S+1}L_J$ level	E (exp.)	E (calc.)	$^{2S+1}L_J$ level	E (exp.)	E (calc.)
$^4I_{9/2}$	0	−11		13 539	13 549	+	21 198	21 184	+	–	30 143
	123	103				$^2K_{15/2}$	21 331	21 311		30 221	30 235
$^2I_{13/2}$	195	320	$^4F_{9/2}$	14 610	14 620		–	21 393	$^2I_{13/2}$	–	30 252
	321	294		14 686	14 692		21 413	21 419		30 391	30 405
	360	367		14 756	14 775		–	21 448		–	30 422
				14 803	14 792		–	21 511		–	30 431
$^4I_{11/2}$	1936	1934		14 839	14 835		21 535	21 524		30 511	30 502
	1977	1996					–	21 572		–	30 532
	2027	2045	$^2H2_{11/2}$	15 844	15 876		21 622	21 641		–	30 558
	2079	2094		15 886	15 887		21 668	21 657		30 641	30 630
	2123	2132	not	15 904	15 902		21 714	21 706		–	30 694
	2183	2181	used	15 980	15 910		–	21 757		–	30 790
			for	16 022	15 931		–	21 777		–	30 865
$^4I_{13/2}$	3908	3891	fit	16 043	15 945		21 805	21 819			
	3965	3955					21 860	21 850	$^2L_{17/2}$	–	31 324
	4009	3997	$^2G1_{7/2}$	16 998	17 038					–	31 397
	4068	4060		17 073	17 072	$^2P_{1/2}$	23 208	23 205		–	31 529
	4102	4096	+	17 166	17 168					–	31 567
	4169	4155		17 240	17 257	$^2D1_{5/2}$	23 657	23 659		–	31 628
	4182	4173	$^4G_{5/2}$	17 285	17 279		23 801	23 785		–	31 692
				17 321	17 314		23 864	23 877		–	31 800
$^4I_{15/2}$	5842	5849		17 442	17 436					–	31 934
	5924	5924				$^2P_{3/2}$	26 069	26 072		–	32 059
	6018	6015	$^4G_{7/2}$	18 882	18 884		26 181	26 177			
	6074	6082		18 957	18 961				$^2H1_{9/2}$	32 685	32 691
	6179	6185		19 002	18 982	$^4D_{3/2}$	27 864	27 854		–	32 701
	6243	6252		19 059	19 056		27 898	27 892		–	32 733
	6270	5274								–	32 820
	6325	6324	$^4G_{9/2}$	19 255	19 303	$^4D_{5/2}$	28 059	28 022		–	32 882
				19 449	19 447		28 233	28 234			
$^4F_{3/2}$	11 410	11 381		19 473	19 463		28 300	28 296			
	11 530	11 485	+	19 490	19 476				$^2D2_{3/2}$	33 191	33 210
				19 515	19 510	$^4D_{1/2}$	28 548	28 577		–	33 285
$^4F_{5/2}$	12 430	12 415	$^2K_{13/2}$	19 535	19 534						
+	12 476	12 450		–	19 566	$^2I_{11/2}$	28 969	28 971	$^2D2_{5/2}$	–	34 012
$^2H2_{9/2}$	12 500	12 539		19 593	19 577		29 066	29 081	+	–	34 044
	12 552	12 559		19 627	19 617		29 143	29 137		–	34 095
	12 620	12 592		19 683	19 665		29 287	29 300	$^2H1_{11/2}$	–	34 138
	12 658	12 644		19 791	19 810		–	29 382		–	34 160
	12 679	12 700		19 840	19 839		29 555	29 528		–	34 203
	12 723	12 737								34 246	34 242
			$^2G1_{9/2}$	20 890	20 878	$^2L_{15/2}$	29 819	29 815		–	34 281
$^4F_{7/2}$	13 367	13 374		–	20 920		–	29 896		–	34 354
+	13 434	13 454	+	20 941	20 957	+	30 062	30 061			
$^4S_{3/2}$	13 501	13 494	$^4G_{11/2}$	20 993	20 976		–	30 062			
	13 501	13 508	+	21 051	21 017	$^4D_{7/2}$	–	30 080			
	13 539	13 521	$^2D1_{3/2}$	21 132	21 144		–	30 091			

The very large $^4F_{3/2}$ splitting (216 cm^{-1}) is one of the largest found in the literature for compounds containing trivalent neodymium. This suggests large values for the B_q^2 cfps, in agreement with the results previously found for Eu^{3+} [5].

Fig. 2 shows the absorption spectra in the region of the so called hypersensitive transition $^4I_{9/2} \rightarrow {}^4G_{5/2}, {}^4G_{7/2}$. The ticked absorption line is not assigned to the trigonal phase, as well as a number of extra lines in other areas. That probably indicates the presence of an unknown phase (probably $Nd_2Si_2O_7$), not detected by the X-ray diffraction technique.

4. Simulation of the energy level scheme

According to the review in Ref. [19], the hamiltonian representing the electronic structure of a $4f^N$ configuration is written as follows:

Table 2
Experimental and calculated energy levels of $NdBSiO_5$

$^{2S+1}L_J$ level	E (exp.)	E (calc.)	$^{2S+1}L_J$ level	E (exp.)	E (calc.)	$^{2S+1}L_J$ level	E (exp.)	E (calc.)	$^{2S+1}L_J$ level	E (exp.)	E (calc.)
$^4I_{9/2}$	0	6		13 810	13 796	$^2K_{15/2}$	21 343	21 325	+	30 521	30 519
	181	176					21 440	21 416		–	30 595
	293	307	$^4F_{9/2}$	14 736	14 721		21 497	21 494	$^2I_{13/2}$	–	30 638
	470	476		14 825	14 848		21 553	21 547		30 642	30 650
	555	562		14 891	14 899		–	21 570		–	30 680
				14 944	14 968		–	21 709		–	30 771
$^4I_{11/2}$	1934	1932		15 078	15 046		21 747	21 756		–	30 849
	2135	2122					21 795	21 801		–	30 893
	2196	2201	$^2H2_{11/2}$	16 022	16 035		21 835	21 826		30 926	30 910
	2225	2243		16 046	16 051		21 904	21 898		–	30 950
	2285	2282	not	16 067	16 077		–	21 915		31 067	31 068
	2320	2334	used	16 104	16 094		21 955	21 951		–	31 074
			for	16 136	16 129		22 006	21 994		–	31 160
$^4I_{13/2}$	3867	3865	fit	16 204	16 175		22 113	22 116	$^2L_{17/2}$	–	31 254
	4087	4074					22 221	22 222		–	31 563
	4150	4151	$^2G1_{7/2}$	17 163	17 195					–	31 829
	4233	4216		17 271	17 274	$^2P_{1/2}$	23 367	23 363		–	32 021
	4268	4260	+	17 388	17 377					–	32 126
	4290	4295		17 454	17 452	$^2D1_{5/2}$	23 767	23 749		–	32 267
	4330	4330	$^4G_{5/2}$	17 496	17 482		23 946	23 957		–	32 466
				17 529	17 536		–	24 209		–	32 585
$^4I_{15/2}$	5776	5786		17 590	17 584						
	6002	5995				$^2P_{3/2}$	26 159	26 186	$^2H1_{9/2}$	–	32 807
	6128	6137	$^4G_{7/2}$	19 052	19 031		–	26 423	+	32 907	32 918
	6273	6268		19 086	19 104				$^2D2_{3/2}$	–	33 061
	6331	6339		19 159	19 151	$^4D_{3/2}$	27 961	27 955		33 113	33 110
	6412	6423		19 224	19 195		28 087	28 088		33 201	33 188
	6476	6482								33 278	33 288
	6533	6537	$^4G_{9/2}$	19 354	19 351	$^4D_{5/2}$	28 221	28 186		33 518	33 552
			+	19 514	19 515		28 487	28 468			
$^4F_{3/2}$	11 494	11 467	$^2K_{13/2}$	19 598	19 623		28 703	28 700	$^2D2_{5/2}$	34 143	34 142
	11 510	11 677		19 633	19 641				+	34 235	34 195
				19 664	19 667	$^4D_{1/2}$	28 885	28 930	$^2H1_{11/2}$	34 281	34 298
$^4F_{5/2}$	12 514	12 496		19 701	16 712					–	34 404
+	12 599	12 629		19 747	19 752	$^2I_{11/2}$	28 885	29 039		34 423	34 426
$^2H2_{9/2}$	12 637	12 650		19 806	19 787		29 236	29 183		34 555	34 536
	12 685	12 694		19 861	19 852	+	29 508	29 258		34 585	34 597
	12 739	12 721		19 930	19 938		29 820	29 406		34 661	34 666
	–	12 828		20 052	20 077	$^2L_{15/2}$	30 139	29 527		34 710	34 706
	12 898	12 913		20 235	20 207		30 521	29 572			
	–	13 002				+	30 642	29 787	$^2F2_{5/2}$	38 552	38 522
			$^2G1_{9/2}$	21 023	21 003		30 926	29 814		–	38 812
$^4F_{7/2}$	13 438	13 447	+	21 038	21 034	$^4D_{7/2}$	31 067	30 029		–	38 974
+	13 573	13 596	$^4G_{11/2}$	21 085	21 064			30 141	$^2F2_{7/2}$	39 956	39 990
$^4S_{3/2}$	13 635	13 655	+	21 118	21 137			30 353		–	40 144
	13 688	13 686	$^2D1_{3/2}$	21 208	21 221			30 393		–	40 200
	13 711	13 707	+	21 264	21 292			30 473		–	40 259

$$H_{FI} = H_0 + \sum_{\nu=0,1,2,3} E^{\nu}(nf, nf)e_{\nu} + \zeta A_{SO} + \alpha L(L+1) + \beta G(G_2) + \gamma G(R_7) + \sum_{\lambda=2,3,4,6,7,8} T^{\lambda} t_{\lambda},$$

in which H_0 represents the spherically symmetric one electron part of the free ion hamiltonian, E^{ν} and ζ the Racah parameters and the spin–orbit coupling constant, respectively, whereas e_{ν} and A_{SO} correspond to the angular part of the operators. For configurations having two or more electrons, α, β and γ are the parameters associated to the two-body correction associated to the angular momentum L and to the Casimir operators G for the groups G_2 and R_7, respectively. For configurations of more than two electrons, the three body correction is parametrized with the Judd parameter, T^{λ}. The standard one-electron crystal field hamiltonian is constituted by a sum of products between the spherical harmonics and the even rank cfps, B_q^k for the real and S_q^k for the imaginary parts, respectively. Its expression is written as follows:

$$H_{CF} = \sum_{k=2}^{4,6} \sum_{q=0}^{k} \left[B_q^k (C_q^k + (-1)^q C_{-q}^k) + iS_q^k (C_q^k - (-1)^q C_{-q}^k) \right].$$

The number of crystal field parameters is limited according to the symmetry of the rare earth point site. As seen from the experimental results listed in Tables 1 and 2, most of the J-manifolds are split in the maximum number of the $(2J+1/2)$ crystal field sublevels. For configurations with an odd number of electrons, this indicates a symmetry lower than cubic. In the present case and according to the crystallographic data, the point symmetry is assumed to be approximated to C_2 or (C_s). Fifteen cfps are then included in the simulation, one of them (S_2^2) being set to zero by an appropriated rotation of the reference axis system.

The complete $4f^3$ configuration is described on the basis of the 364 $|^{2S+1}L_{JM}>$kets, corresponding to 182 Kramers' doublets. All interactions are included together in the secular determinant, before diagonalization [20].

The refinement is carried out by taking into account the 109 experimental levels for $NdBGeO_5$ (respectively, 125 for $NdBSiO_5$). The procedure is conducted by minimizing the r.m.s. standard deviation taken as a figure of merit. However, due to the relatively great number of parameters, the simulation procedure is conducted in three steps; (i) in the first step the cfps (real and imaginary parts are fixed to the values found for Eu^{3+} in the corresponding matrix [5]), only the free ion parameters vary, except γ whcih is almost always fixed to its standard value; (ii) in the second step the free ion parameters are now fixed and the cfps vary; (iii) in the last step almost all parameters vary freely.

The results are presented in Table 3. The cfps only have a few differences with those determined for Eu^{3+}, as expected in an isostructural series. In spite of a relatively great number of phenomenological parameters, the r.m.s. is good, but smaller for $NdBSiO_5$ than for $NdBGeO_5$. This allows a good agreement between experimental and calculated energy levels, in all of the explored spectral domain, including the $^2H_{11/2}$ level which often presents large discrepancies in the simulation.

Table 3
Phenomenological crystal field parameters for Nd^{3+} in $NdBGeO_5$ and $NdBSiO_5$

Parameter	$NdBGeO_5$	$NdBSiO_5$
E^0	23 543.57	23 769
E^1	4778.96	4841.35
E^2	23.42	23.54
E^3	483.92	482.70
α	21.33	20.92
β	−608.66	−609.54
γ	1548.44	1305.91
T^2	284.06	366.57
T^3	34.28	38.45
T^4	105.11	92.53
T^6	−280.27	−264.85
T^7	341.59	325.59
T^8	317.23	319.80
ζ	875.65	875.81
B_0^2	−637	−233
B_2^2	94	1015
S_2^2	–	0
B_0^4	327	949
B_2^4	−1162	−167
S_2^4	–	450
B_4^4	−444	350
S_4^4	–	−598
B_0^6	−462	−369
B_2^6	167	851
S_2^6	–	−458
B_4^6	214	−8
S_4^6	–	510
B_6^6	517	103
S_6^6	–	−194
Number of levels	109	125
σ	17.5	18.1

5. Conclusion

The absorption spectra as well as the simulation of the energy levels schemes of $NdBGeO_5$ and $NdBSiO_5$ confirms that the substitution of Si by Ge gives another structural type. The crystal field is very different in the stillwellite-like structure from the datolite one, especially through high second rank crystal field parameters in the former case. Of course, the phenomenological simulation of the energy level sequences does not permit the direct explanation of the particular optical properties of $La_{1-x}RE_xBGeO_5$ (RE = Pr, Nd). It gives an expression of the wavefunctions of the levels, which is necessary to manipulate when transition probabilities are studied. In such a case, it should not be possible to parameterize the transition intensities because of the very large number of

parameters, a consequence of the low symmetry. However, this type of simulation provides good wavefunctions for intensity calculation from semiempirical models.

References

[1] K.B. Belabaev, A.A. Kaminskii, S.E. Sarbisov, Phys. Stat. Sol. (a) 28 (1975) K17.
[2] V.G. Dimitriev, E.V. Raevskii, N.M. Rubina, Zh. Tekh. Fiz. Pisma 5 (1979) 1400.
[3] L.M. Dorozhkin, I.I. Kuratev, N.I. Leonyuk, Tekh. Fiz. Pisma 7 (1981) 1297.
[4] A.A. Kaminskii, A.A. Butashin, I.A. Maslyanizin, B.V. Mill, V.S. Mironov, S.P. Rosov, S.E. Sarkisov, V.D. Shigorin, Phys. Stat. Sol. (a) 125 (1991) 671.
[5] E. Antic-Fidancev, S. Serhan, M. Taïbi, M. Lemaitre-Blaise, P. Porcher, J. Aride, A. Boukhari, J. Phys.: Condens. Mater. 6 (1994) 6857.
[6] E. Antic-Fidancev, M. Lemaitre-Blaise, P. Caro, J. Chem. Phys. 73 (1980) 4613.
[7] B. Piriou, D. Fahmi, J. Dexpert-Ghys, A. Taitai, J.L. Lacout, J. Lumin. 39 (1987) 97.
[8] International Tables for Crystallography, Kluwer Academic Publishers, 1993.
[9] J. McAndrew, T.R. Scott, Nature 176 (1955) 509.
[10] P. Gay, Miner. Mag. 31 (1967) 465.
[11] A.A. Voronkov, Yu.A. Pyatenko, Crystallography 12 (1967) 214.
[12] A. Callegari, G. Giuseppetti, F. Mazzi, C. Tadini, Neu. Jahn. Miner. Monats. (Germany) 0 (1992) 49.
[13] A. Rulmont, P. Tarte, J. Solid State Chem. 75 (1988) 244.
[14] G.V. Lysanova, B.F. Dzhurinskii, M.G. Komova, Izv. Akad. Nauk. SSSR, Ser. Neorg. Mater. 25 (1989) 632.
[15] A.A. Kaminskii, B.V. Mill, E.L. Belokonova, A.V. Butashin, Izv. Akad. Nauk. SSSR, Ser. Neorg. Mater. 26 (1990) 1105.
[16] E.L. Belokonova, B.V. Mill, A.V. Butashin, A.A. Kaminskii, Izv. Akad. Nauk. SSSR, Ser. Neorg. Mater. 27 (1991) 556.
[17] P. Caro, J. Derouet, Bull. Soc. Chim. Fr. 1 (1972) 46.
[18] E. Antic-Fidancev, M. Lemaitre-Blaise, P. Caro, New J. Chem. 11 (1987) 467.
[19] W.T. Carnall, G.L. Goodman, K. Rajnak, R.S. Rana, J. Chem. Phys. 90 (1989) 3443.
[20] P. Porcher, FORTRAN programs REEL and IMAGE for simulation of the nd^N and nf^N electronic configurations involving real and complex crystal field parameters (1989) (unpublished).